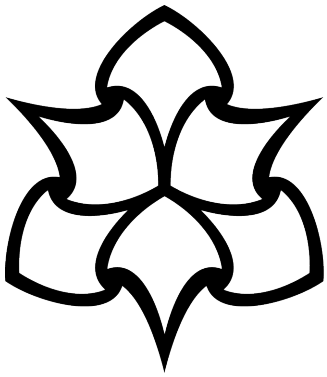

Journal of Environmental Chemical Engineering 9 (2021) 106046

Contents lists available at ScienceDirect

Journal of Environmental Chemical Engineering

journal homepage: www.elsevier.com/locate/jece

# The effect of $TiO_2$ coatings on the formation of ozone and nitrogen oxides in non-thermal atmospheric pressure plasma

Samuel C. Capp, David A.G. Sawtell, Craig E. Banks, Peter J. Kelly, Zaenab Abd-Allah *

*Faculty of Science and Engineering, Manchester Metropolitan University, John Dalton Building, Manchester M15 6BH, United Kingdom*

ARTICLE INFO

Editor: Dr. G. Palmisano

*Keywords:*
Plasma chemistry
Photocatalyst
Packed bed reactor
Titanium dioxide
Ozone
Nitrogen oxides

ABSTRACT

The use of photocatalytic materials in plasma systems has the potential to enhance the selectivity and yield of desired products. However, the surface interaction between the photocatalyst and plasma is a complex process that is not well understood. This work presents a comprehensive study of the effects of combining titanium dioxide ($TiO_2$) photocatalysts with non-thermal atmospheric pressure nitrogen-oxygen plasmas, which increases the production of ozone and dinitrogen pentoxide ($N_2O_5$) while limiting the formation of harmful nitrogen dioxide ($NO_2$) and nitrous oxide ($N_2O$) by products. $TiO_2$ coatings were deposited by magnetron sputtering onto barium titanate ($BaTiO_3$) particulates for use within a packed bed dielectric barrier discharge reactor (DBD). The presence of titanium dioxide can affect the plasma chemistry in the DBD by acting as a sink for atomic oxygen, through photocatalytic formation of superoxide anion radical ($O_2^-$), and alteration of the dielectric constant of the $BaTiO_3$ particulates. This work explains the complex interaction of these effects on oxygen and nitrogen plasma chemistry. The effect of the photocatalyst surface properties, gas composition and residence time on the reaction pathways for the formation of ozone and nitrogen oxides ($N_xO_y$) were investigated. The photocatalytic activity of titanium dioxide was improved by annealing the coated surface, and was subsequently found to enable the formation of ozone, increase the formation of $N_2O_5$ while significantly decreasing the formation of harmful $NO_2$ and $N_2O$ with a residence time of 0.011 s

## 1. Introduction

Recent years have seen a large emphasis on heterogeneous photocatalysis in the literature due to its potential for environmental and energy related applications [1–4]. Titanium dioxide has received a large amount of interest since the discovery of its light induced water splitting properties in the 1970 s [5]. $TiO_2$ is a well-known photocatalyst and semiconductor with a band gap of 3.2 eV. Photons with a high enough energy are absorbed by electrons and can cause the electrons to be promoted from the valence band to the conduction band, resulting in the creation of electron hole pairs, which can lead to reduction and oxidation reactions [6]. $TiO_2$ has three main crystal phases, anatase, rutile and brookite, with anatase being the most photocatalytically active phase [7]. Furthermore, tailoring of the morphology of the $TiO_2$, either through the use of porous structures [8], or the tailoring of nanoparticle size and shape [9], can increase it's photocatalytic activity.

Non-thermal plasma, often referred to as 'cold' plasma, is produced at low, or atmospheric pressure by devices such as the dielectric barrier discharge, which consists of two electrodes separated by a dielectric material [10,11]. One of the main advantages of non-thermal plasma is the ability to produce chemically active species at reduced temperatures and as such, these types of plasmas are used for chemical synthesis and the degradation of pollutants, in addition to many other applications [12,13]. Photocatalysts are activated by photons of sufficient energy and as plasma emits photons of ultraviolet and visible radiation, plasma has the potential to activate photocatalytic materials, thus improving yield and selectivity of plasma based chemical reaction processes. The combination of photocatalyst and non-thermal plasma has received significant interest in recent years due to its potential for increasing product yields and energy efficiency in a variety of processes [14–17] The underlying mechanisms of combining catalysts and plasma are not completely understood however, as the plasma can modify the catalyst surface, in turn, the presence of the catalyst can affect the plasma properties, and so further investigation into the interaction between the

*Abbreviations:* UV, Ultraviolet; NO, Nitric Oxide; SED, Specific Energy Density; FTIR, Fourier Transform Infrared Spectroscopy; XPS, X-ray Photoelectron Spectroscopy; SEM, Scanning Electron Microscopy.

* Corresponding author.
*E-mail address:* z.abd-allah@mmu.ac.uk (Z. Abd-Allah).

https://doi.org/10.1016/j.jece.2021.106046
Received 1 June 2021; Received in revised form 6 July 2021; Accepted 10 July 2021
Available online 13 July 2021

two is required.

Ozone is an oxidant that sees widespread use in water treatment due to its being effective in sterilization of bacteria and viruses. The production of harmful nitrogen oxides is unavoidable when using air plasma for the formation of ozone. However, plasma photocatalysis presents a promising approach to increase ozone selectivity. $N_2O_5$ is an environmentally friendly nitrating agent and an industrially significant precursor chemical that is used for manufacturing a range of energetic polymeric materials, explosives and propellants [18].

Pekárek et.al [19] reported the use of $TiO_2$ and ZnO in a surface dielectric barrier discharge for the production of ozone from air. They found that the concentration of ozone increased slightly when using $TiO_2$ and ZnO, compared to when no catalyst was used. $TiO_2$ catalysts have also been investigated for their effect on $N_xO_y$ reaction pathways and production yields. Jõgi et.al [20] produced ozone using a coaxial dielectric barrier discharge and investigated the effect of $TiO_2$ on ozone induced oxidation of NO to $NO_2$ and $N_2O_5$. At high temperatures the $TiO_2$ catalyst was found to improve the efficiency of oxidation of $NO_2$ to $N_2O_5$.

One potentially viable method of adding the photocatalyst to non-thermal plasma is through surface coating of components of the DBD. Magnetron sputtering is a widely used technique for producing high quality thin films onto a variety of substrates. The use of magnetron sputtering to produce alloys and doped films allows for the production of tailored photocatalytic thin films [21,22]. Magnetron sputtering is a widely used technique in which the deposition parameters can be precisely controlled. This, in turn, allows for a high degree of control over the final properties of the films produced [23]. Furthermore, magnetron sputtering allows for adjusting the morphology of the coated $TiO_2$ [24], increasing the surface area and improving photocatalytic activity [25].

The underlying mechanisms of the interaction between plasma and photocatalyst for the formation of ozone and $N_xO_y$ species is still not fully understood, and this work aims to address this gap in literature. For this work, $TiO_2$ coatings were deposited onto the surface of a packing material of a packed bed DBD. The packing material used in this case was barium titanate particulates (1–3 mm diameter), which was placed in-between the two electrodes. Magnetron sputtered $TiO_2$ coatings with different photocatalytic activities were deposited onto the $BaTiO_3$ particulates in order to assess the effect of photocatalysis on the formation of ozone and nitrogen oxides in an oxygen and nitrogen discharge. This novel approach of combining plasma and photocatalyst aims to improve the interaction between the catalyst and non-thermal plasma, allowing the photocatalyst to be activated by UV and light photons, whilst also being in direct contact with active species produced within the plasma region. Moreover, introducing the photocatalysts as a thin film coating on the packing material eliminates any disturbance to the gas flow through the DBD.

## 2. Experimental

### 2.1. Thin film deposition

$TiO_2$ coatings were deposited onto $BaTiO_3$ dielectric particulates for use within a packed bed DBD reactor. All coatings were deposited using a 300 mm × 100 mm planar unbalanced type II magnetron with a titanium target of 99.5% purity, located in a vacuum chamber which was pumped down to a base pressure of $1 \times 10^{-3}$ Pa. The magnetron was installed through the chamber roof in a sputter down configuration. The reactive sputtering process was carried out in an argon and oxygen atmosphere. A dual channel Advanced Energy Pinnacle Plus power supply operated in pulsed DC mode was used to power the magnetron. Deposition runs were carried out; with a frequency of 150 kHz, a duty cycle of 50% and power of 1000 W for the deposition of titania. The flows of oxygen and argon were controlled using mass flow controllers and fixed to 11.5 sccm and 15 sccm, respectively. A deposition time of 3 h was performed for all coatings.

The deposition process for the $TiO_2$ photocatalyst onto $BaTiO_3$ particulates was carried out using a bespoke oscillating bowl for the uniform coating of the particulates. The bowl oscillates vertically with springs connected between the electromagnet and the base plate which also impart a lateral twisting moment to the oscillation. The resulting motion causes particles in the bowl to roll or hop in a circular path around the bottom of the bowl and, thus, over time all surfaces of the particles are exposed to the coating flux. The design of the oscillator is described in detail in previous work [3,26]. In order to obtain an anatase phase of $TiO_2$, heat treatment of the coated $BaTiO_3$ particulates was performed for an hour at 500 °C in an air filled muffle furnace, model Carbolite 3000 [27].

### 2.2. Surface characterisation

To assess the topography of the coatings on the particulates, scanning electron microscopy (SEM) measurements were performed with a JEOL JSM-5600LV SEM. To assess the chemical composition of the coatings, Raman spectroscopy was performed on the coated and uncoated particulates using a Thermo scientific DXR Raman microscope with a 532 nm laser at 1 mW, 50x LWD microscope, 900 line per mm grating, an estimated spot size of 1.1 μm and a 25 μm pinhole, in order to determine the crystalline structure of the $TiO_2$. To further probe the chemical composition of the coatings, X-ray photoelectron spectroscopy was performed on the coated and uncoated particulates with an AMICUS photoelectron spectrometer (Kratos analytical AXIS Supra+) equipped with Mg K X-rays as the primary excitation source. The binding energy was referenced to the C 1s line at 284.8 eV for calibration. Curve fitting was performed applying a Gaussian function with a Shirley background.

The photocatalytic activity of all used particulates was assessed using a dye degradation test, to establish the difference in photocatalytic activity between uncoated $BaTiO_3$, as-deposited $TiO_2$-coated and annealed $TiO_2$-coated $BaTiO_3$. Methylene blue was chosen due to its frequent use in testing for photocatalytic activity [28–31]. 1.5 g of $BaTiO_3$ particulates were used per test. An Ocean Optics DH-2000-BAL UV–VIS–NIR spectrometer, UV-A source (2 × 15 W Sankyo Denki black light blue lamps, peaked at 365 nm) and Spectrasuite software, which measures and displays the absorption of light passing through the cuvette dye solution, were used. Particulates were placed within a covered cuvette (40 × 40 mm) with 50 mL of methylene blue solution (2 μmol/L) and left in the dark until the absorption of methylene blue on the surface of the particulates was in equilibrium with the methylene blue in solution. Subsequently, the samples were radiated by UV light and the degradation of methylene blue was measured for 2 h. The characteristic wavelength of the absorption peak of methylene blue dye which was measured is at 664.11 nm. The increase in light passing through the solution is proportional to the degradation of the methylene blue dye. The pseudo-first-order rate constant $k_\alpha$ was obtained from the gradient of the plot, $\ln(A_o/A_t)$ against time, where $A_o$ is the absorbance at the start (time equals zero) and $A_t$ is the absorbance at time, t. The obtained $k_\alpha$ values were used to compare the photocatalytic activity of each sample [32].

The stability of the $TiO_2$ coating in terms of the production of final products was considered. Experiments were repeated over several days, ozone and $N_xO_y$ concentrations did not show significant variation. Averages of repeated measurements are presented in Figs. 8 and 9. Previous work by the group [32,33] showed a good durability and usability of $TiO_2$ coating produced using magnetron sputtering.

### 2.3. Packed bed reactor experimental conditions

The packed bed reactor consists of two stainless steel circular mesh electrodes, separated by $BaTiO_3$ dielectric packing particulates, and enclosed by a 30 mm inner diameter Pyrex tube. Stainless steel funnels at the entrance and outlet of the packed bed DBD were used to uniformly distribute and collect the gases entering and exiting the reactor. A 12.5

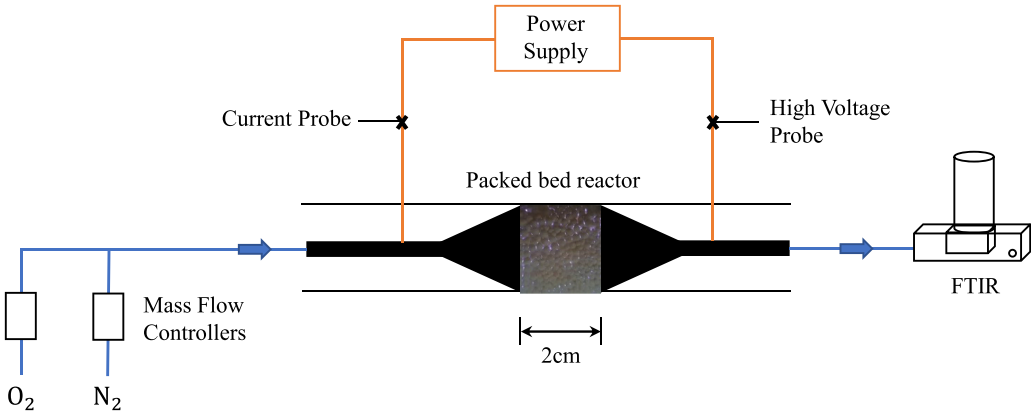


**Fig. 1.** Schematic of the experimental setup.

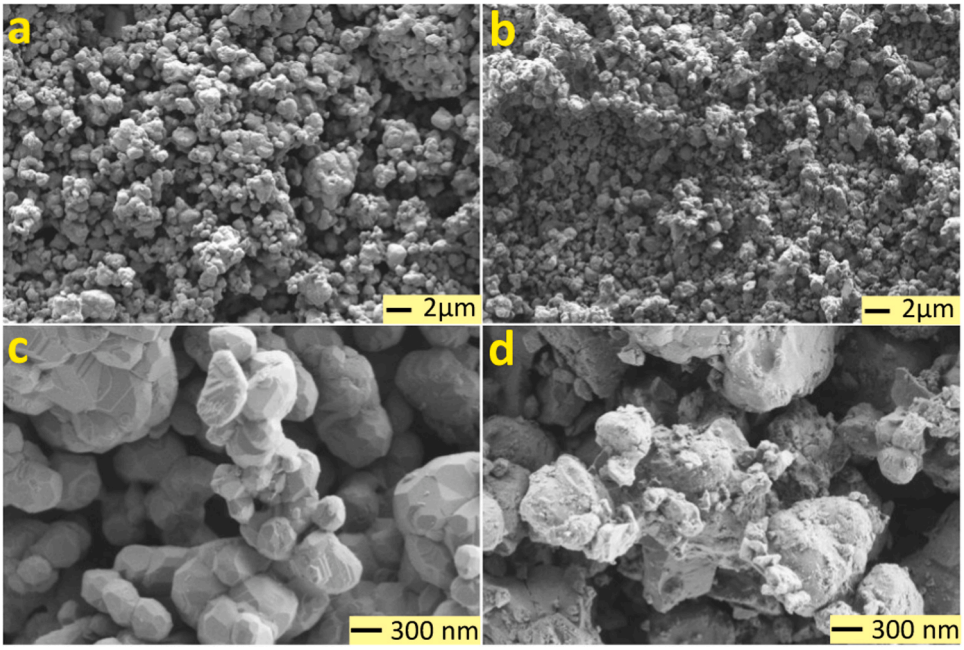


**Fig. 2.** SEM images of - (a) $BaTiO_3$ particulates with no coating. (b) $BaTiO_3$ particulates with $TiO_2$ coating. (c) $BaTiO_3$ particulates with no coating and 10 times increased magnification. (d) $BaTiO_3$ particulates with $TiO_2$ coating and 10 times increased magnification.

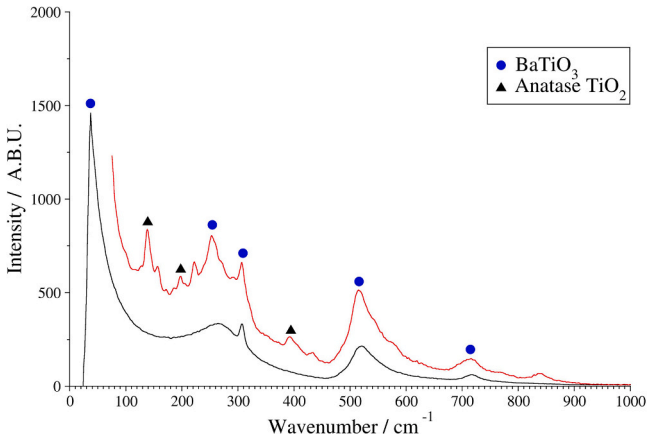


**Fig. 3.** Raman spectra of – (black line) uncoated $BaTiO_3$ particulate. (red line) annealed $TiO_2$-coated $BaTiO_3$ particulate for an hour at 500 °C in an air-filled muffle furnace. (For interpretation of the references to colour in this figure legend, the reader is referred to the web version of this article.)

$cm^3$ packing volume was used for all experiments, with both coated and uncoated $BaTiO_3$ particulates being investigated. The power supply is detailed in previous research [34]. Current and voltage measurements were made with a Pearson 4100 current monitor and a Tektroniks 1000:1 voltage probe and were recorded on a Tektronix MDO 3014 digital oscilloscope. Applied power was calculated from the current and voltage measurements, and was kept constant at 15 W, with a peak to peak voltage of 8.6 kV and a frequency of 16 kHz. A total flow rate of 1–3 standard liters per minute (SLM), resulting in a residence time of 0.0111 s and 0.0037 s respectively was used. The nitrogen and oxygen gases were used as delivered with a purity of 99.999% and 99.5% respectively. The concentration of oxygen was varied from 3% to 21% in 3% increments and was controlled by MKS mass flow controllers. Fig. 1 shows a schematic of the experimental setup.

### 2.4. Gas analysis

A Perkin Elmer Spectrum Two Fourier Transform Infrared Spectroscopy with a Specac Tornado 5 m path length gas cell, situated about 1 m away from the reactor, was used to qualify and quantify the exhaust

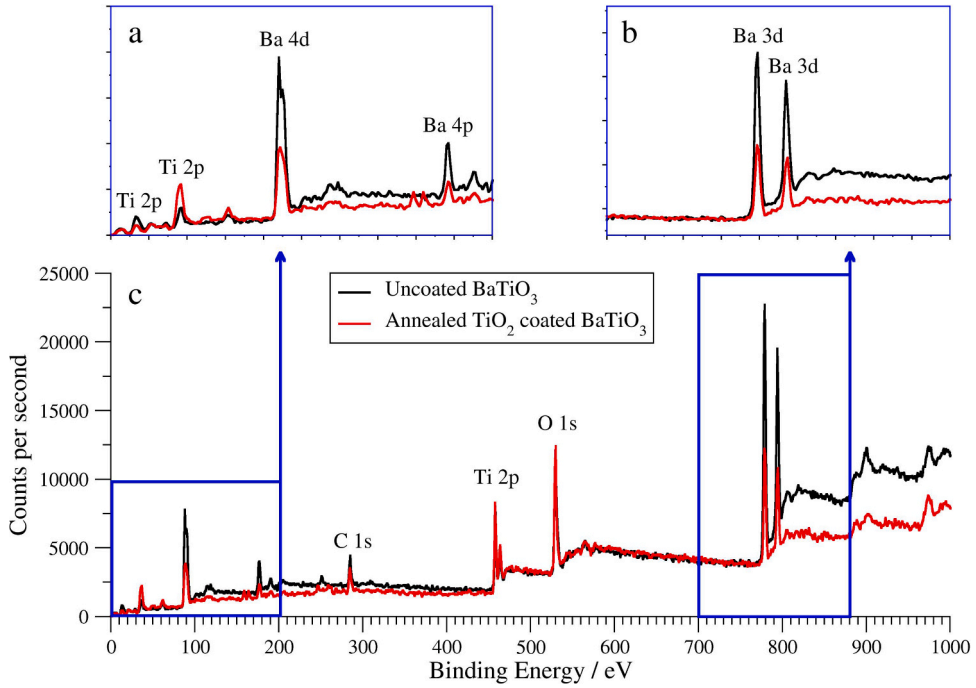


**Fig. 4.** XPS measurements of uncoated $BaTiO_3$ and annealed $TiO_2$ coated $BaTiO_3$ particulates, a and b are magnified spectra for the highlighted ranges in c.

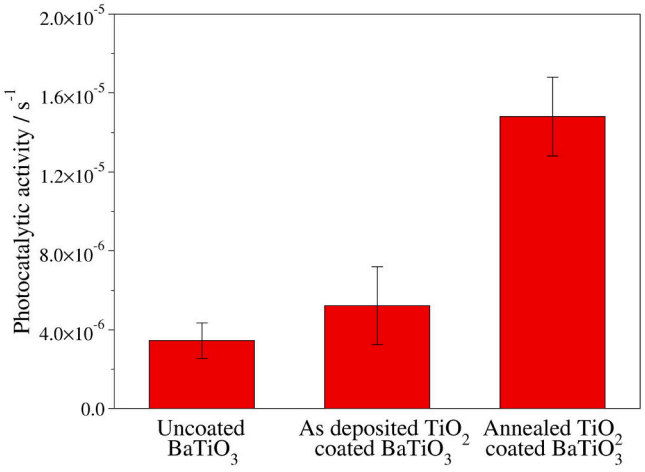


**Fig. 5.** Photocatalytic activity of various samples as determined from the degradation of methylene blue dye.

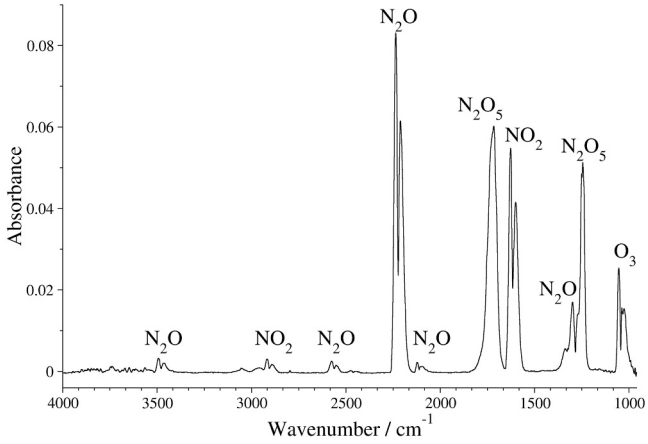


**Fig. 6.** Example FTIR spectra for air plasma after the packed bed plasma reactor with a peak to peak voltage of 8.6 kV, a frequency of 16 kHz and a total flow rate of 1 SLM and annealed $TiO_2$ coated $BaTiO_3$ packing material.

gases from the packed bed reactor. A spectral resolution of 4 $cm^{-1}$ with 5 averages per scan was used. The system was flushed with nitrogen and oxygen and allowed to reach a steady state before measurements were commenced. Once the plasma was initiated, three measurements were taken at equally spaced intervals and results were averaged. The concentrations of ozone and nitrogen oxides were determined by integrating the area under each absorbance band using MatLab and then comparing these areas to those obtained from integration between similar limits from standard spectra database and literature. Standard spectra for ozone was obtained from National Institute of Standards and Technology (NIST) [35]. Pacific Northwest National Laboratory (PNNL) database [36] was used to obtain standard spectra for $NO_2$ and $N_2O$. The concentration of $N_2O_5$ was calculated with reference to work done by Fitzsimmons et al. [37].

## 3. Results and discussion

### 3.1. Surface characterisation

SEM images presented in Fig. 2 show the surface of the $BaTiO_3$ particulates before and after coating. Fig. 2A and C show the surface of uncoated $BaTiO_3$ at different magnifications, while B and D show the surface of the $TiO_2$ coated $BaTiO_3$ beads, at different magnifications. Fig. 2A shows that the surface of the $BaTiO_3$ particulates compromises of small micro particles, this is due to the process of forming the particulates from powder by CATAL International Ltd.

Raman spectroscopy was used to verify the presence of anatase $TiO_2$ on the surface of the coated particulates. Anatase peaks were only found on the surface of annealed particulates as shown in Fig. 3. Characteristic anatase peaks could be seen at 144 $cm^{-1}$, 197 $cm^{-1}$ and 399 $cm^{-1}$ [38]. No anatase peaks were observed on the surface of uncoated $BaTiO_3$ particulates. As-deposited $TiO_2$ coated particulates showed a similar

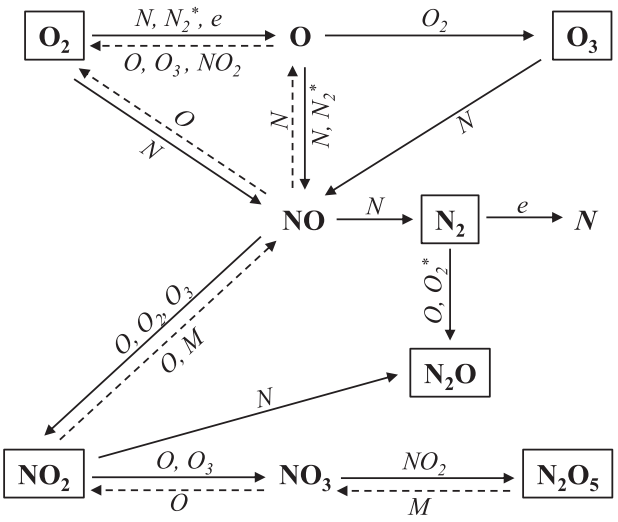


**Fig. 7.** Reaction pathways for the formation of ozone and $N_xO_y$ species in air plasma.

spectrum to that of uncoated particulates.

X-ray photoelectron spectroscopy was carried out on 100 μm by 100 μm areas to analyse the stoichiometry of the surface of the particulates and enable an understanding of the role that the surface coatings could play in non-thermal plasma experiments. Fig. 4 shows the XPS spectra for uncoated $BaTiO_3$ and annealed $TiO_2$ coated $BaTiO_3$. The spectra show a clear increase in the signal of Ti 3p orbitals for $TiO_2$ coated $BaTiO_3$ particulates and a strong decrease in signal of Ba 4d, 4p and 3d orbitals. This illustrates an increase in surface coverage of Ti compared to Ba due to the $TiO_2$ coating.

### 3.2. Photocatalytic activity

Fig. 5 shows the photocatalytic activity of the uncoated $BaTiO_3$ and with $TiO_2$ coating, both as-deposited and annealed. As-deposited $TiO_2$ coated $BaTiO_3$ particulates showed little increase in photocatalytic activity compared to the uncoated sample due to the fact that there was no heat treatment performed to obtain the photocatalytic active phase of anatase. The annealed particulates showed photocatalytic activity, with an average reaction rate constant of $1.4 \times 10^{-5}$ $s^{-1}$, with 2.8 times increase in photocatalytic activity compared to the as-deposited $TiO_2$ coated $BaTiO_3$ sample. This is in-line with findings in Fig. 3, illustrating that further treatment of the $TiO_2$ coated particulates is required to produce the photocatalytically active anatase phase.

### 3.3. Effect on plasma chemistry

The effect of photocatalytic coatings on plasma chemistry was investigated using the packed-bed plasma reactor with the formation of ozone and nitrogen oxides in flowing oxygen and nitrogen gas mixtures being investigated. Fig. 6 shows a typical FTIR spectrum of the outlet gases from an air plasma generated in the packed bed dielectric barrier discharge. The main end products detected are $NO_2$, $N_2O$, $N_2O_5$ and ozone. The formation of energetic electrons, active nitrogen and oxygen species in the plasma region [39–43]leads to a complex reaction scheme resulting in the formation of the end products seen in the FTIR spectrum.

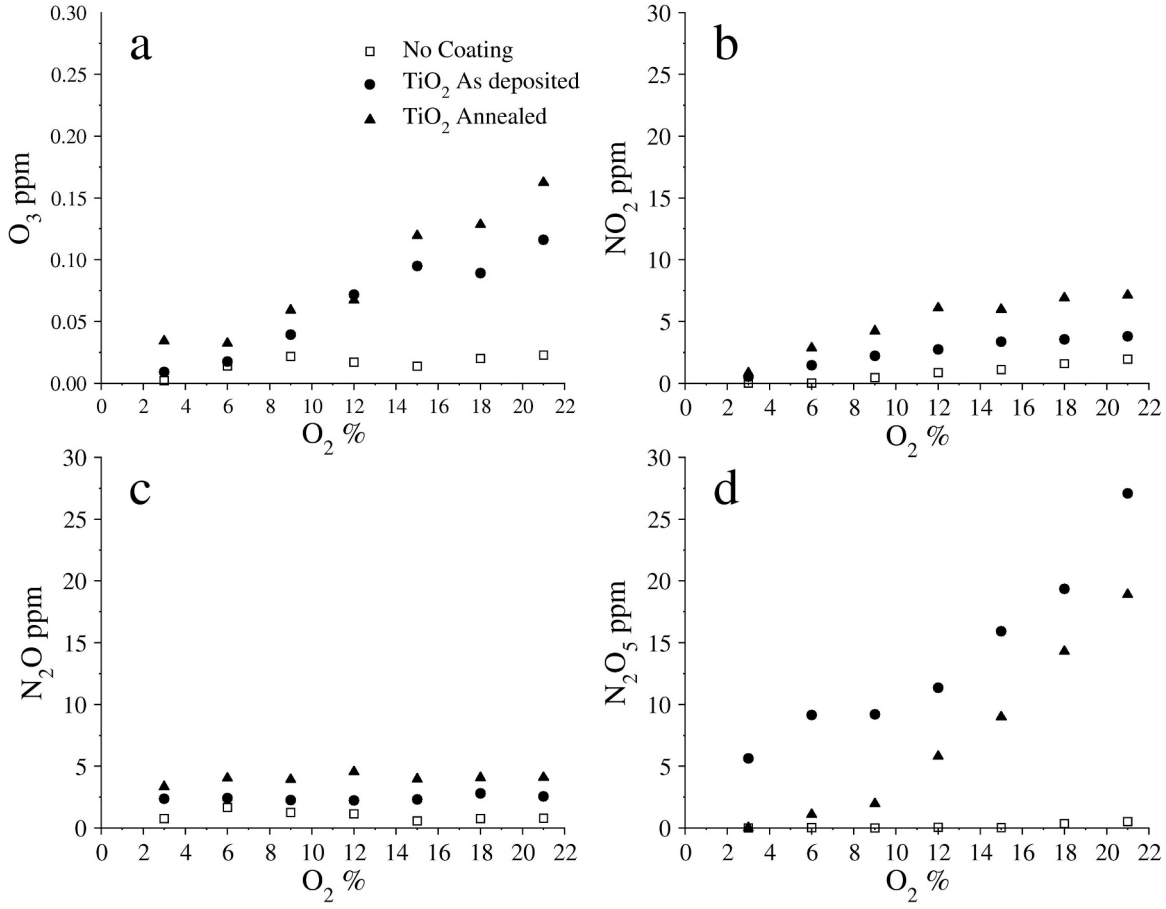


**Fig. 8.** Effects of oxygen concentration on a) ozone production b) $NO_2$ production, c) $N_2O$ production and d) $N_2O_5$ production for uncoated, coated, and coated and annealed $BaTiO_3$ packing material at a residence time of 0.0037 s, specific energy density of 0.3 kJ/L and an applied power of 15 watts.

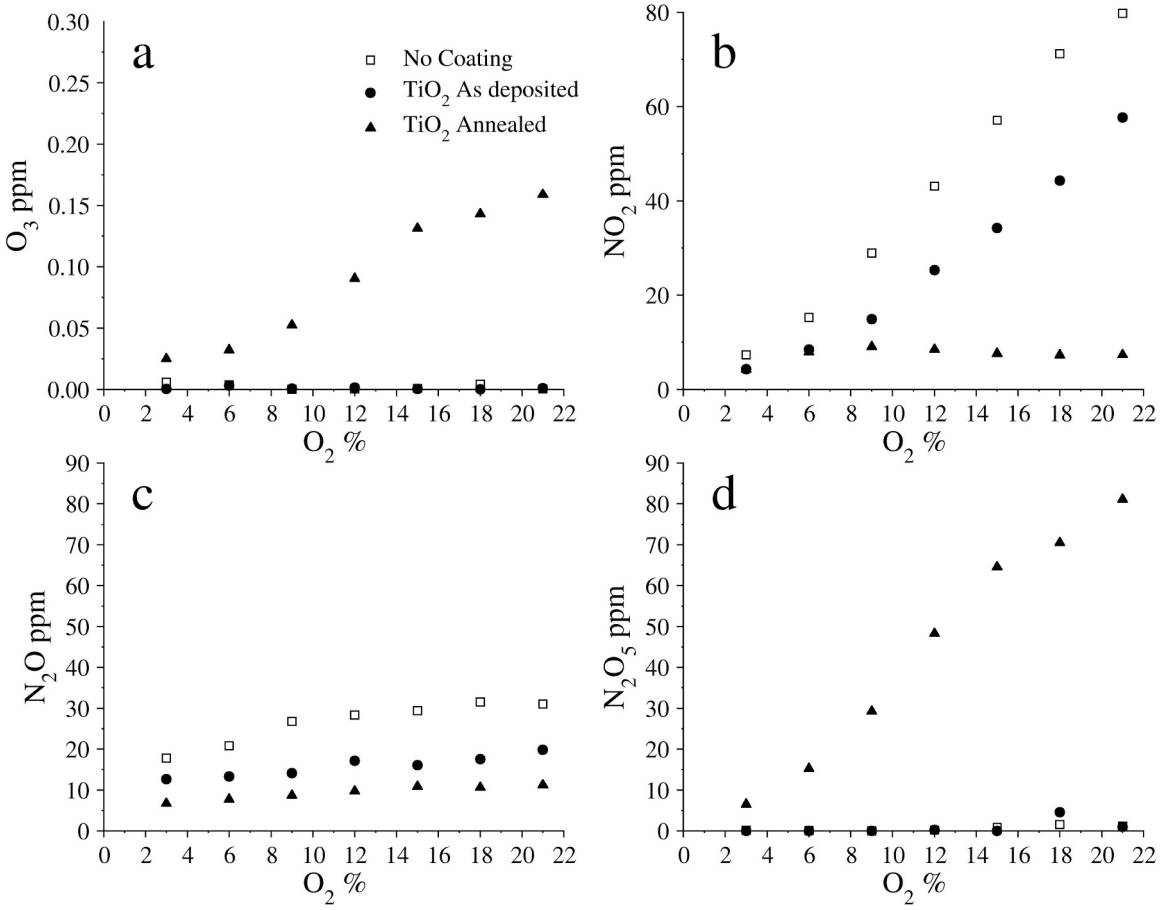


**Fig. 9.** Effects of oxygen concentration on a) ozone production b) $NO_2$ production, c) $N_2O$ production and d) $N_2O_5$ production for uncoated, coated, and coated and annealed $BaTiO_3$ packing material at a residence time of 0.011 s, specific energy density of 0.9 kJ/L and an applied power of 15 watts.

A simplified reaction scheme for the production of nitrogen and oxygen species using atmospheric pressure plasmas was developed with reference to literature [37,39,43–48] and is shown in Fig. 7.

The effect of coating conditions and gas residence time on the production of ozone and nitrogen oxides species was investigated and results are presented in Figs. 8 and 9.

Fig. 8 represents the effect of uncoated, as-deposited $TiO_2$-coated and annealed $TiO_2$-coated $BaTiO_3$ on the formation of ozone and nitrogen oxides as a function of oxygen concentration in oxygen-nitrogen plasmas. The total flow rate was set to 3 SLM, giving a residence time of gases in the plasma region of 0.0037 s and specific energy density of 0.3 kJ/L. SED is calculated by dividing the applied power by the total flow rate. The applied power was measured as the total power supplied to the packed-bed plasma reactor; this is not to be confused with plasma power.

Results show that negligible concentrations of ozone and nitrogen oxide species were detected with uncoated $BaTiO_3$ particulates. However, increased concentrations of all these species were observed with the use of $TiO_2$ coated particulates indicating modification of the plasma chemistry as a result of plasma surface interaction.

Fig. 8-a shows the effect of oxygen concentration and coating conditions on the formation of ozone. Ozone is mainly produced in non-thermal plasmas by a two stage reaction scheme with the collision of oxygen and electrons followed by the three body reaction as seen in Eqs. (1) and (2) [49].

$$O_2 + e \rightarrow 2O + e \quad (1)$$

$$O + O_2 + O_2 \rightarrow O_3 + O_2 \quad (2)$$

In the case of uncoated $BaTiO_3$, small concentrations of ozone generation were detected in the outlet gases of the plasma reactor. The dielectric constant for $BaTiO_3$ is in the range of 5000–15000, this leads to the formation of a strong electric field at the contact points between the particulates, which is thought to cause the decomposition of any ozone that is generated in the plasma [12]. Various studies, as summarized by Chen et al. [46], confirm that particulates with too high dielectric constants can cause the decomposition of ozone, it is theorized that hot spots at the contact points between the particulates cause this decomposition.

A clear increase in ozone concentration was observed when the $BaTiO_3$ was coated with $TiO_2$. It is thought that this is due to the reduced dielectric constant of the coated particulates. $TiO_2$ has a much lower dielectric constant, in the range of 17–64 [50], compared to $BaTiO_3$. As a result, the electric field at the contact points between the coated particulates is reduced, which in turn reduces the decomposition of ozone at these contact points. Moreover, in the presence of photocatalytically active annealed $TiO_2$, the formation of ozone is thought to be further enhanced due to the generation of $O_2^-$ [51], via the following reaction [49,52].

$$O_2^- + O \rightarrow O_3 + e^- \quad (3)$$

In the case of the as-deposited $TiO_2$, both the lack of $O_2^-$ production, and the oxygen vacancies present at the surface of the particulates, which act as a sink for the atomic oxygen, reduces the rate of production of ozone in comparison to using photocatalytically active annealed $TiO_2$-coated $BaTiO_3$. The oxygen vacancies are significantly reduced when the $TiO_2$ has been annealed in air, and the vacancies have been filled. With both annealed and as-deposited $TiO_2$ coated beads, ozone concentration

increased with increasing oxygen concentration as a result of increased production of active oxygen molecules and atoms in the plasma region leading to increased formation of ozone as described in Eqs. (1) and (2).

Fig. 8-b,c and d show the effect of oxygen concentration and coating conditions on the formation of $NO_2$, $N_2O$ and $N_2O_5$ respectively. An increase of the concentration of all $N_xO_y$ species was noticed with $TiO_2$ coated particulates compared to uncoated particulates. This is mainly due to the formation of ozone, as explained earlier, which activates the pathways to the formation of NO, $NO_2$ and subsequently the formation of $N_2O$ and $N_2O_5$ as explained in the reaction pathway in Fig. 6. Furthermore, the formation of $N_2O_5$ reduces the final concentration of $NO_2$ and $N_2O$ as $N_2O_5$ is mainly formed via a two-stage reaction scheme consuming $NO_2$, limiting the amount of $NO_2$ available to react with nitrogen atoms and form $N_2O$ [53].

The effect of increasing the residence time of gases in the plasma region was investigated and results are shown in Fig. 9. The total flow rate was reduced to 1 SLM, giving a residence time of gases in the plasma region of 0.011 s and SED of 0.9 kJ/L. The effect of the coating conditions and oxygen concentration with the increased residence time was investigated.

Again, a clear difference in the concentration of ozone and nitrogen oxide species can be seen as a result of coating conditions, indicating that plasma chemistry was modified as a result of plasma surface interaction. Ozone and $N_2O_5$ were only detected with annealed $TiO_2$-coated $BaTiO_3$ as shown in Fig. 9-a and d respectively. The formation of ozone in the presence of photocatalytically active annealed $TiO_2$-coated $BaTiO_3$, is a direct result of the formation of $O_2^-$ species as explained previously. Negligible concentration of ozone was detected with uncoated and as-deposited $TiO_2$ coated $BaTiO_3$. The effect of the strong electric field at the contact points of the particulates, in the case of uncoated $BaTiO_3$, and the effect of the oxygen vacancies on the surface of the as-deposited $TiO_2$-coated $BaTiO_3$ is thought to be increased with increased residence time. The longer residence time of the gases in the plasma leads to more decomposition of ozone at the contact points of the uncoated particulates, and an increased consumption of atomic oxygen at the oxygen vacancies on the surface of the as-deposited $TiO_2$-coated particulates. As the formation of $N_2O_5$ is directly linked to the formation of ozone via a two-stage reaction scheme with $NO_2$ to form $NO_3$, followed by further reactions between $NO_3$ and $NO_2$ to form $N_2O_5$ [53], no formation was detected with uncoated and as-deposited $TiO_2$ coated $BaTiO_3$.

The formation of $NO_2$ and $N_2O$ shown in Fig. 9-b and c showed an increased concentration with uncoated $BaTiO_3$ and as-deposited $TiO_2$-coated $BaTiO_3$ compared to annealed $TiO_2$-coated $BaTiO_3$. This is a direct result of the absence of ozone related chemical pathway reactions that lead to the formation of $N_2O_5$, limiting the amount of $NO_2$ available to react with nitrogen atoms and form $N_2O$. Furthermore, in the case of as-deposited $TiO_2$, the concentration of $NO_2$ and $N_2O$ were less than that with uncoated $BaTiO_3$. This is a result of the oxygen vacancies on the surface of the as-deposited $TiO_2$, leading to a reduced availability of atomic oxygen that could react with NO and $N_2$ to form $NO_2$ and $N_2O$ respectively.

Results showed an increase in the formation of $NO_2$ and $N_2O$ with increased residence time when uncoated and as-deposited $TiO_2$-coated particulates were used. When the residence time is increased, more active species were formed in the plasma, increasing the chemical reactions taking place, and subsequently causing further formation of $NO_2$ and $N_2O$. The concentration of all detected species increased with increasing concentration of oxygen, this is a direct result of increased formation of active oxygen molecules and atoms in the plasma region leading to increased formation of end products.

Increasing the residence time by mean of reducing the total flow rate, leads to an increase of the SED. It is reported that increasing the SED in air plasma leads to increased concentrations of $NO_2$ and $N_2O$, which in turn stops the formation of ozone. Increasing the SED leads to fast reactions of oxygen atoms with $NO_x$ forming NO and $NO_2$ and subsequently $N_2O$, an effect known as discharge poisoning [47]. Our results for uncoated and as-deposited $TiO_2$-coated particulates are in agreement with these findings. However, the presence of photocatalytically active annealed $TiO_2$-coated $BaTiO_3$ stopped the effect of discharge poisoning with increased SED. No increase in the concentration of $NO_2$ and $N_2O$ was observed. The increase in $N_2O_5$ concentration after the reactor must be a result of increased ozone formation within the reactor. This again proves that photocatalyst have a significant effect on plasma chemistry. More investigations are required to further understand the role that the photocatalysts play in stopping the discharge poisoning effect in air plasma.

In summary, increasing the residence time of gases in the plasma region allowed for the formation of more active species per unit volume, resulting in further chemical reactions taking place both in the gas phase and due to the gas-catalyst surface interaction.

## 4. Conclusion

A comprehensive study of the effects of combining photocatalytic materials with plasma on the plasma chemistry of nitrogen and oxygen mixtures has been carried out. In this case, $TiO_2$ coatings were deposited by magnetron sputtering onto $BaTiO_3$ particulates and used in a packed bed dielectric barrier discharge. The presence of $TiO_2$ on the surface of the packing material affects the plasma chemistry through acting as an atomic oxygen sink, photocatalytic formation of $O_2^-$, and modification of the dielectric constant of the $BaTiO_3$ particulates. The photocatalytic activity of the coated particulates was improved by annealing the $TiO_2$, which enabled the formation of the anatase phase. The results show that the anatase phase is responsible for the improved production of desired products, $O_3$ and $N_2O_5$ through the photocatalytic formation of $O_2^-$ species, which enhanced the formation of ozone via reaction (3). This in turn resulted in enhanced formation of $N_2O_5$ through the two-stage reaction scheme consuming $NO_2$ and subsequently limiting the formation of $N_2O$. The increase in $N_2O_5$ formation in the presence of annealed $TiO_2$, opens up a potential new route for synthesis of this industrially significant chemical. Moreover, the presence of photocatalytically active annealed $TiO_2$-coated $BaTiO_3$, stopped the effect of discharge poisoning with increased SED. The findings of this study show that it is possible to tailor the plasma chemistry of nitrogen and oxygen mixtures through the modification of the plasma facing materials and surfaces, optimising yields of ozone and $N_2O_5$ whilst limiting the formation of harmful by-products.

## Funding

Samuel C Capp received a Faculty of Science and Engineering Ph.D. studentship funded by Manchester Metropolitan University. Research was also supported by the Research Accelerator grant, Manchester Metropolitan University.

## CRediT authorship contribution statement

**Samuel C Capp**: Investigation, Methodology, Validation, Writing – original draft. **David A G Sawtell**: Conceptualization, Writing – review & editing, Visualization, Supervision. **Craig E Banks:** Writing – review & editing, Supervision. **Peter J Kelly:** Resources, Writing – review & editing, Supervision. **Zaenab Abd-Allah:** Conceptualization, Writing – review & editing, Visualization, Supervision.

## Declaration of Competing Interest

The authors declare that they have no known competing financial interests or personal relationships that could have appeared to influence the work reported in this paper.

## Acknowledgement

The authors would like to thank Dr Hayley Andrews and Dr Gary Miller for their technical support in using the SEM and XPS. Thanks also to Dr. David Glover the founder and technical director of Plasma Clean LTD for all the useful discussions.

## References

[1] K.M. Lee, C.W. Lai, K.S. Ngai, J.C. Juan, Recent developments of zinc oxide based photocatalyst in water treatment technology: a review, Water Res. 88 (Suppl C) (2016) 428–448, https://doi.org/10.1016/j.watres.2015.09.045.

[2] S. Varnagiris, M. Urbonavicius, S. Tuckute, M. Lelis, D. Milcius, Development of photocatalytically active $TiO_2$ thin films on expanded polystyrene foam using magnetron sputtering, Vacuum 143 (2017) 28–35, https://doi.org/10.1016/j.vacuum.2017.05.031.

[3] M. Ratova, B.R. Marcelino, P.P. de Souza, C.C. Amorim, J.P. Kelly, Reactive magnetron sputter deposition of bismuth tungstate coatings for water treatment applications under natural sunlight, Catalysts 7 (10) (2017) 283, https://doi.org/10.3390/catal7100283.

[4] V. Kumaravel, S. Mathew, J. Bartlett, S.C. Pillai, Photocatalytic hydrogen production using metal doped $TiO_2$: a review of recent advances, Appl. Catal. B Environ. 244 (2019) 1021–1064, https://doi.org/10.1016/j.apcatb.2018.11.080.

[5] A. Fujishima, K. Honda, Electrochemical photolysis of water at a semiconductor electrode, Nature 238 (5358) (1972) 37–38, https://doi.org/10.1038/238037a0.

[6] K. Nakata, A. Fujishima, $TiO_2$ photocatalysis: design and applications, J. Photochem. Photobiol. C Photochem. Rev. 13 (3) (2012) 169–189, https://doi.org/10.1016/j.jphotochemrev.2012.06.001.

[7] C.P. Lin, H. Chen, A. Nakaruk, P. Koshy, C.C. Sorrell, Effect of annealing temperature on the photocatalytic activity of $TiO_2$ thin films, Energy Procedia 34 (2013) 627–636, https://doi.org/10.1016/j.egypro.2013.06.794.

[8] J.H. Pan, H.Q. Dou, Z.G. Xiong, C. Xu, J.Z. Ma, X.S. Zhao, Porous photocatalysts for advanced water purifications, J. Mater. Chem. 20 (22) (2010) 4512–4528, https://doi.org/10.1039/b925523k.

[9] Y.F. Li, Z.P. Liu, Particle size, shape and activity for photocatalysis on titania anatase nanoparticles in aqueous surroundings, J. Am. Chem. Soc. 133 (39) (2011) 15743–15752, https://doi.org/10.1021/ja206153v.

[10] X. Xu, Dielectric barrier discharge — properties and applications, Thin Solid Films 390 (1–2) (2001) 237–242, https://doi.org/10.1016/S0040-6090(01)00956-7.

[11] U. Kogelschatz, Dielectric-barrier discharges: their history, discharge physics, and industrial applications, Plasma Chem. Plasma Process. 23 (1) (2003) 1–46, https://doi.org/10.1023/A:1022470901385.

[12] Z. Abd Allah, J.C. Whitehead, P. Martin, Remediation of dichloromethane ($CH_2Cl_2$) using non-thermal, atmospheric pressure plasma generated in a packed-bed reactor, Environ. Sci. Technol. 48 (1) (2014) 558–565, https://doi.org/10.1021/es402953z.

[13] Z.A. Allah, J.C. Whitehead, Plasma-catalytic dry reforming of methane in an atmospheric pressure AC gliding arc discharge, Catal. Today 256 (Part 1) (2015) 76–79, https://doi.org/10.1016/j.cattod.2015.03.040.

[14] D.H. Mei, X.B. Zhu, C.F. Wu, B. Ashford, P.T. Williams, X. Tu, Plasma-photocatalytic conversion of $CO_2$ at low temperatures: understanding the synergistic effect of plasma-catalysis, Appl. Catal. B Environ. 182 (2016) 525–532, https://doi.org/10.1016/j.apcatb.2015.09.052.

[15] W.A. Saoud, A.A. Assadi, M. Guiza, S. Loganathan, A. Bouzaza, W. Aboussaoud, A. Ouederni, S. Rtimi, D. Wolbert, Synergism between non-thermal plasma and photocatalysis: implicationsin the post discharge of ozone at a pilot scale in a catalytic fixed-bed reactor, Appl. Catal. B Environ. 241 (2019) 227–235, https://doi.org/10.1016/j.apcatb.2018.09.029.

[16] S. Meng, A. Wang, P. He, H. Song, Nonthermal plasma-assisted photocatalytic conversion of simulated natural gas for high-quality gasoline production near ambient conditions, J. Phys. Chem. Lett. 11 (10) (2020) 3877–3881, https://doi.org/10.1021/acs.jpclett.0c00934.

[17] V. Palma, M. Cortese, S. Renda, C. Ruocco, M. Martino, E. Meloni, A review about the recent advances in selected nonthermal plasma assisted solid–gas phase chemical processes, Nanomaterials 10 (8) (2020), https://doi.org/10.3390/nano10081596.

[18] R.W. Millar, M.E. Colclough, A.W. Arber, R.P. Claridge, R.M. Endsor, J. Hamid, ChemInform abstract: clean nitrations using dinitrogen pentoxide ($N_2O_5$) - a UK perspective, ChemInform 42 (12) (2011).

[19] S. Pekárek, J. Mikeš, J. Krýsa, Comparative study of $TiO_2$ and ZnO photocatalysts for the enhancement of ozone generation by surface dielectric barrier discharge in air, Appl. Catal. A Gen. 502 (2015) 122–128, https://doi.org/10.1016/j.apcata.2015.06.003.

[20] I. Jõgi, K. Erme, J. Raud, M. Laan, Oxidation of NO by ozone in the presence of $TiO_2$ catalyst, Fuel 173 (2016) 45–51, https://doi.org/10.1016/j.fuel.2016.01.039.

[21] M. Ratova, G.T. West, P.J. Kelly, Photocatalytic visible-light active bismuth tungstate coatings deposited by reactive magnetron sputtering, Vacuum 115 (Suppl C) (2015) 66–69, https://doi.org/10.1016/j.vacuum.2015.02.008.

[22] P. Panyajirawut, N. Pratumsuwan, K. Meesombad, K. Thanawattana, A. Chingsungnoen, N. Boonyopakorn, M. Aiempanakit, W. Pecharapa, Preparing transparent cobalt-doped ZnO thin films by DC magnetron sputtering, Mater. Today Proc. 4 (5, Part 2) (2017) 6311–6316, https://doi.org/10.1016/j.matpr.2017.06.132.

[23] P. Navabpour, S. Ostovarpour, J. Hampshire, P. Kelly, J. Verran, K. Cooke, The effect of process parameters on the structure, photocatalytic and self-cleaning properties of $TiO_2$ and Ag-$TiO_2$ coatings deposited using reactive magnetron sputtering, Thin Solid Films 571 (2014) 75–83, https://doi.org/10.1016/j.tsf.2014.10.040.

[24] M. Ratova, D. Sawtell, P.J. Kelly, Micro-patterning of magnetron sputtered titanium dioxide coatings and their efficiency for photocatalytic applications, Coatings 10 (1) (2020) 68, https://doi.org/10.3390/coatings10010068.

[25] W. Zhou, W. Li, J.Q. Wang, Y. Qu, Y. Yang, Y. Xie, K.F. Zhang, L. Wang, H.G. Fu, D. Y. Zhao, Ordered mesoporous black $TiO_2$ as highly efficient hydrogen evolution photocatalyst, J. Am. Chem. Soc. 136 (26) (2014) 9280–9283, https://doi.org/10.1021/ja504802q.

[26] M. Ratova, P.J. Kelly, G.T. West, L. Tosheva, M. Edge, Reactive magnetron sputtering deposition of bismuth tungstate onto titania nanoparticles for enhancing visible light photocatalytic activity, Appl. Surf. Sci. 392 (Suppl C) (2017) 590–597, https://doi.org/10.1016/j.apsusc.2016.09.035.

[27] Y.-Q. Hou, D.-M. Zhuang, G. Zhang, M. Zhao, M.-S. Wu, Influence of annealing temperature on the properties of titanium oxide thin film, Appl. Surf. Sci. 218 (1–4) (2003) 98–106, https://doi.org/10.1016/S0169-4332(03)00569-5.

[28] A. Houas, H. Lachheb, M. Ksibi, E. Elaloui, C. Guillard, J.-M. Herrmann, Photocatalytic degradation pathway of methylene blue in water, Appl. Catal. B Environ. 31 (2) (2001) 145–157, https://doi.org/10.1016/S0926-3373(00)00276-9.

[29] L. Andronic, A. Enesca, C. Vladuta, A. Duta, Photocatalytic activity of cadmium doped $TiO_2$ films for photocatalytic degradation of dyes, Chem. Eng. J. 152 (1) (2009) 64–71, https://doi.org/10.1016/j.cej.2009.03.031.

[30] Saepurahman, M.A. Abdullah, F.K. Chong, Dual-effects of adsorption and photodegradation of methylene blue by tungsten-loaded titanium dioxide, Chem. Eng. J. 158 (3) (2010) 418–425, https://doi.org/10.1016/j.cej.2010.01.010.

[31] R.S. Dariani, A. Esmaeili, A. Mortezaali, S. Dehghanpour, Photocatalytic reaction and degradation of methylene blue on $TiO_2$ nano-sized particles, Opt. Int. J. Light Electron Opt. 127 (18) (2016) 7143–7154, https://doi.org/10.1016/j.ijleo.2016.04.026.

[32] M. Grao, M. Ratova, C.C. Amorim, R.B.P. Marcelino, P. Kelly, Crystalline $TiO_2$ supported on stainless steel mesh deposited in a one step process via pulsed DC magnetron sputtering for wastewater treatment applications, J. Mater. Res. Technol. 9 (3) (2020) 5761–5773, https://doi.org/10.1016/j.jmrt.2020.03.101.

[33] M. Grao, M. Ratova, P. Kelly, Design and optimisation of a low-cost titanium dioxide-coated stainless steel mesh photocatalytic water treatment reactor, J. Clean. Prod. 297 (2021), 126641, https://doi.org/10.1016/j.jclepro.2021.126641.

[34] D.A.G. Sawtell, Z. Abd-Allah, J.W. Bradley, G.T. West, P.J. Kelly, Mechanisms of atmospheric pressure plasma treatment of BOPP, Plasma Process. Polym. 15 (1) (2018), 1700051, https://doi.org/10.1002/ppap.201700051.

[35] A.L. Smith. The Coblentz Society Desk Book of Infrared Spectra in Carver, Second ed., The Coblentz Society, Kirkwood, MO, 1982.

[36] S. Sharpe, T. Johnson, R. Sams, P. Chu, G. Rhoderick, P. Johnson, Gas-phase databases for quantitative infrared spectroscopy, Appl. Spectrosc. 58 (12) (2004) 1452–1461, https://doi.org/10.1366/0003702042641281.

[37] C. Fitzsimmons, J.T. Shawcross, J.C. Whitehead, Plasma-assisted synthesis of $N_2O_5$ from $NO_2$ in air at atmospheric pressure using a dielectric pellet bed reactor, J. Phys. D Appl. Phys. 32 (10) (1999) 1136–1141, https://doi.org/10.1088/0022-3727/32/10/310.

[38] T. Ohsaka, F. Izumi, Y. Fujiki, Raman spectrum of anatase, $TiO_2$, J. Raman Spectrosc. 7 (6) (1978) 321–324, https://doi.org/10.1002/jrs.1250070606.

[39] B.M. Penetrante, M.C. Hsiao, J.N. Bardsley, B.T. Merritt, G.E. Vogtlin, A. Kuthi, C. P. Burkhart, J.R. Bayless, Identification of mechanisms for decomposition of air pollutants by non-thermal plasma processing, Plasma Sour. Sci. Technol. 6 (3) (1997) 251–259, https://doi.org/10.1088/0963-0252/6/3/002.

[40] K. Takaki, J.S. Chang, K.G. Kostov, Atmospheric pressure of nitrogen plasmas in a ferro-electric packed bed barrier discharge reactor - part I: modeling, IEEE Trans. Dielectr. Electr. Insul. 11 (3) (2004) 481–490, https://doi.org/10.1109/tdei.2004.1306726.

[41] H.H. Kim, Nonthermal plasma processing for air-pollution control: a historical review, current issues, and future prospects, Plasma Process. Polym. 1 (2) (2004) 91–110, https://doi.org/10.1002/ppap.200400028.

[42] Z. Abd-Allah, D.A.G. Sawtell, G.T. West, P.J. Kelly, J.W. Bradley, Mass spectrometric observations of the ionic species in a double dielectric barrier discharge operating in nitrogen, Plasma Process. Polym. 13 (6) (2016) 649–653, https://doi.org/10.1002/ppap.201500149.

[43] A.C. Gentile, M.J. Kushner, Reaction chemistry and optimization of plasma remediation of NxOy from gas streams, J. Appl. Phys. 78 (3) (1995) 2074–2085, https://doi.org/10.1063/1.360185.

[44] A. Gal, M. Kurahashi, M. Kuzumoto, An energy-consumption and byproduct-generation analysis of the discharge nonthermal plasma-chemical NO-reduction process, J. Phys. D Appl. Phys. 32 (10) (1999) 1163–1168, https://doi.org/10.1088/0022-3727/32/10/313.

[45] J.T. Herron, D.S. Green, Chemical kinetics database and predictive schemes for nonthermal humid air plasma chemistry. Part II. Neutral species reactions, Plasma Chem. Plasma Process. 21 (3) (2001) 459–481, https://doi.org/10.1023/a:1011082611822.

[46] H.L. Chen, H.M. Lee, S.H. Chen, M.B. Chang, Review of packed-bed plasma reactor for ozone generation and air pollution control, Ind. Eng. Chem. Res. 47 (7) (2008) 2122–2130, https://doi.org/10.1021/ie071411s.

[47] A. Fridman. Plasma Chemistry, illustrated, Reprint ed., Cambridge University Press, 2008.

[48] E. Vervloessem, M. Aghaei, F. Jardali, N. Hafezkhiabani, A. Bogaerts, Plasma-based $N_2$ fixation into NOx: insights from modeling toward optimum yields and energy costs in a gliding arc plasmatron, ACS Sustain. Chem. Eng. 8 (26) (2020) 9711–9720, https://doi.org/10.1021/acssuschemeng.0c01815.

[49] B. Eliasson, M. Hirth, U. Kogelschatz, Ozone synthesis from oxygen in dielectric barrier discharges, J. Phys. D Appl. Phys. 20 (11) (1987) 1421–1437, https://doi.org/10.1088/0022-3727/20/11/010.

[50] A. Wypych, I. Bobowska, M. Tracz, A. Opasinska, S. Kadlubowski, A. Krzywania-Kaliszewska, J. Grobelny, P. Wojciechowski, Dielectric properties and characterisation of titanium dioxide obtained by different chemistry methods, J. Nanomater. 2014 (2014) 1–9, https://doi.org/10.1155/2014/124814.

[51] Y. Nosaka, A.Y. Nosaka, Generation and detection of reactive oxygen species in photocatalysis, Chem. Rev. 117 (17) (2017) 11302–11336, https://doi.org/10.1021/acs.chemrev.7b00161.

[52] K. Yanallah, F. Pontiga, A. Fernandez-Rueda, A. Castellanos, Experimental investigation and numerical modelling of positive corona discharge: ozone generation, J. Phys. D Appl. Phys. 42 (6) (2009), 065202, https://doi.org/10.1088/0022-3727/42/6/065202.

[53] X. Tang, J. Wang, H. Yi, S. Zhao, F. Gao, C. chu, Nitrogen fixation and NO conversion using dielectric barrier discharge reactor: identification and evolution of products, Plasma Chem. Plasma Process. 38 (3) (2018) 485–501, https://doi.org/10.1007/s11090-018-9876-4.